Synthesis, Structure, and Thermoelectric Properties of the New Antimonide Sulfide $MoSb_2S$

Chi-Shen Lee[a] and Holger Kleinke*[a]

Keywords: Antimony / Sulfur / Materials science / Chalcogens / Molybdenum

The structure of a new ternary compound, $MoSb_2S$, was identified by single-crystal X-ray diffraction. The title compound was synthesized by heating the elements in stoichiometric ratios in sealed silica tubes at 600–800 °C using small amounts of I_2 as a mineralizator. The compound crystallizes in a new structure type in the monoclinic space group *C*2/*m* [*a* = 36.157(3) Å, *b* = 6.3823(5) Å, *c* = 6.5379(5) Å, β = 95.093(2)°, *Z* = 16, *R*1/*wR*2 = 0.035/0.059]. Its crystal structure contains CdI_2-related layers (MoSbS) and Sb columns, namely a zigzag (*cis-trans*) chain and an equidistant ladder, both of which are located between the MoSbS layers. The results of thermoelectric measurements and electronic structure calculations indicate metallic properties.

Introduction

Thermoelectric materials exhibit a unique property, namely the conversion of heat into electrical energy and vice versa. Such materials, which are usually small-gap semiconductors, have been utilized in applications like refrigerators and power generators. Commercial materials include semiconductors based on Bi_2Te_3, $Si_{0.7}Ge_{0.3}$, and PbTe.[1] Extensive research activities were carried out with investigations of new thermoelectric materials, including the filled skutterudites LnM_4Sb_{12} (Ln = lanthanoid; M = Fe, Co, Ni, ...) and most recently the ternary telluride $CsBi_4Te_6$.[2–5] Good thermoelectric materials have a high *figure-of-merit* that combines a high Seebeck coefficient, low thermal conductivity, and high electrical conductivity. To approach the goal of preparing new thermoelectrics, heavy main group metalloid elements such as antimony, selenium or tellurium may be used as the common element.

Our group has focused on the syntheses and characterizations of new materials in the ternary M–Sb–Q systems (M = transition metal atoms; Q = S, Se, Te). During the course of this study, a new ternary compound, $MoSb_2Se$, was identified.[6] The structure of $MoSb_2Se$ can be treated as the combination of a CdI_2-related layer structure (MoSbSe layer) with interstitial Sb chains binding the Sb atoms of MoSbSe layers. A similar structure is realized in the Mo–Sb–S system; the structure of $MoSb_2S$ exhibits topologically equivalent MoSbS layers, yet significant differences in the Sb atom substructure. With this contribution, the synthesis, characterization and electronic structure studies of $MoSb_2S$ are presented.

[a] Department of Chemistry, University of Waterloo
Waterloo, ON, N2L 3G1, Canada,
Fax: (internat.) + 1-519/746-0435
E-mail: kleinke@uwaterloo.ca

Results and Discussion

Structure

$MoSb_2S$ crystallizes in the space group *C*2/*m*, with six independent positions for Sb, three for Mo, and three for S atoms. The perspective view of the $MoSb_2S$ crystal structure along [010] is illustrated in Figure 1. In general, the structure of $MoSb_2S$ contains a CdI_2-related layer of the composition MoSbS and two types of columnar Sb atom substructures, which bind the Sb atoms of the two surrounding MoSbS layers. Pseudo-octahedral voids remain present in the interlayer Sb atom substructure.

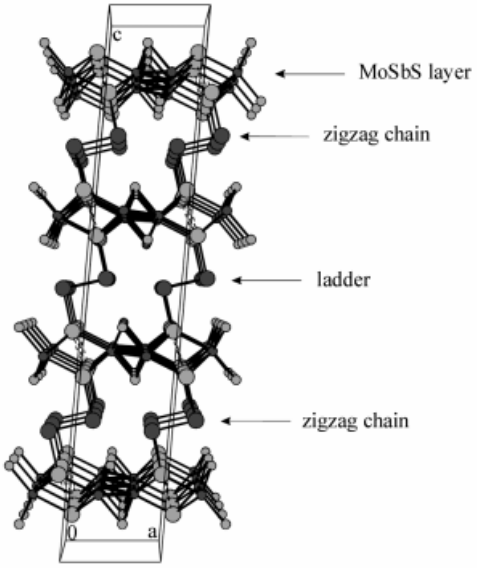

Figure 1. The three-dimensional structure of $MoSb_2S$ projected along [010]; dark circles: Mo; small gray circles: S; large circles: Sb, with dark circles representing interlayer and bright circles intralayer atoms

The Mo atoms are sandwiched between the approximately closed packed Sb and S atom layers, forming MoSbS layers that are reminiscent of the $MoTe_2$ layers of the monoclinic β-$MoTe_2$ [7] structure. Each Mo is coordinated by three Sb and three S atoms in a distorted octahedral coordination. The averaged Mo−Sb and Mo−S distances are 2.83 and 2.38 Å, respectively. This may be compared to the corresponding interatomic distances in Mo_3Sb_7 (d_{Mo-Sb} = 2.77 and 2.85 Å)[8] and MoS_2 (d_{Mo-S} = 2.41 Å).[9]

The Mo atoms in $MoSb_2S$ are connected to form zigzag chains along the *b* axis, as is the case for the β-$MoTe_2$ structure. The shortest Mo−Mo distances are 2.76−2.77 Å, shorter than that of the topologically equivalent chains of $MoSb_2Se$ (2.81 Å) and β-$MoTe_2$ (2.89−2.90 Å). The Mo−Mo bonds in elemental molybdenum (cubic body-centered packing, W type) are 8 × 2.73 and 6 × 3.15 Å per Mo atom. Thus, the Mo−Mo interactions in $MoSb_2S$ have significant bonding character.

The Sb−Sb distances within the MoSbS layer are between 3.18 and 3.33 Å. While these distances are larger than a typical Sb−Sb single bond (2.80−2.90 Å), they are shorter than the weak bond in elemental antimony (d = 3.35 Å). Interactions like these are typically weakly bonding.[10] The averaged S−S and S−Sb distances are 3.19 and 3.64 Å, respectively. These presumably nonbonding contacts are much longer than the sums of the covalent radii (r_S = 1.02, r_{Sb} = 1.40 Å).[11] A detailed discussion of the bonding character of these interactions will be given in the electronic structure section.

Chains comprising Sb atoms are running along the *b* axis between the MoSbS layers. Two types of interlayer Sb−Sb chains exist in the structure of $MoSb_2S$. The first type (located at *x* close to 1/4 and 3/4 as shown in Figure 2a) is a zigzag chain with Sb−Sb bonds of 2.84 (parallel to *b*) and 2.88 Å (approximately parallel to *c*), which are both in the range of the Sb−Sb single bond lengths, as comparisons with KSb (2.83 and 2.85 Å),[12] *cyclo*-Sb_5^{5-} (2.81−2.91 Å),[13] and Sb_{11}^{3-} (2.76−2.85 Å) reveal.[14] Short (2.84 Å) and long (3.54 Å) Sb−Sb distances alternate along [010]. This type of *cis-trans* chain is also found in the structure of $MoSb_2Se$ (Figure 2b). Furthermore, each Sb atom of the zigzag chain binds an Sb atom of the MoSbS layer (d = 2.84 Å). Thus, each Sb atom of the zigzag chain takes part in three Sb−Sb interactions described best as single bonds.

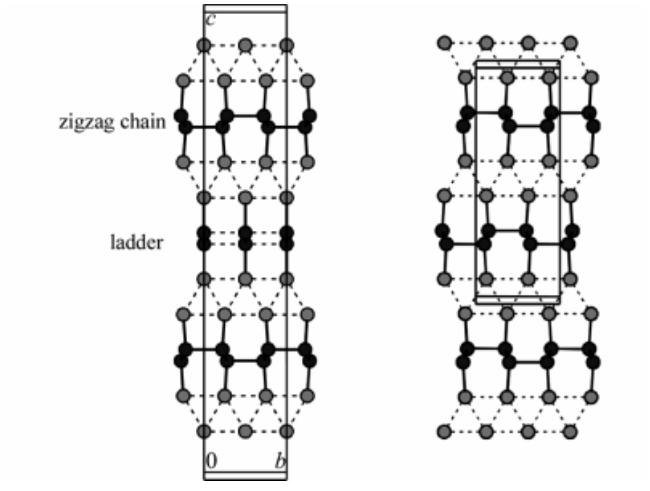

Figure 2. The pseudo two-dimensional Sb atom network of a) $MoSb_2S$ and b) $MoSb_2Se$; solid lines: short Sb−Sb contacts (2.8−2.9 Å); dash lines: long Sb−Sb contact (3.1−3.4 Å)

The second type is an Sb ladder at *x* close to 1/2. Each ladder contains two parallel Sb atom columns with equidistant Sb−Sb contacts of 3.19 Å parallel to the *b* axis. These two columns are interconnected to form the ladder by Sb−Sb bonds of 2.85 Å, and to the Sb atoms of the MoSbS layer by a second Sb−Sb single bond of 2.84 Å. This particular Sb atom substructure is not observed in the $MoSb_2Se$ structure, but the Sb atom ladder compares well to that found in $FeSb_2$ with Sb−Sb distances of 3.20 Å in the columns and 2.89 Å for the bonds connecting the columns to the ladder.[15] Figure 3 illustrates the different columnar Sb atom substructures of $MoSb_2S$, namely the *cis-trans* chain and the ladder.

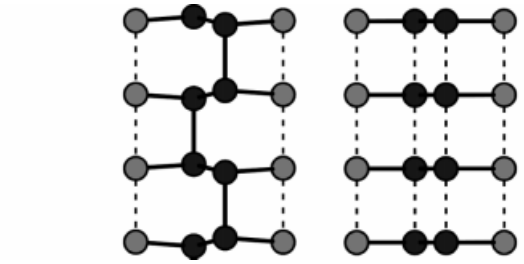

Figure 3. The columnar Sb atom substructure of $MoSb_2S$: a) zigzag chain; b) ladder

Sb−Sb bonds of 3.0−3.2 Å are usually identified as half bonds.[16−21] Instead of forming three full Sb−Sb bonds like the Sb atoms of the zigzag chain, each Sb atom of the ladder forms two full and two half Sb−Sb bonds. This bonding situation resembles those of the $FeSb_2$ structure and of the Li_2Sb structure. In the latter, two different linear Sb atom chains occur; one comprises equidistant Sb−Sb distances of 3.26 Å, and the second one has alternating short and long distances of 2.97 and 3.56 Å.[22]

The question remains, why two different columnar Sb atom substructures occur in $MoSb_2S$, but not in $MoSb_2Se$. In general, the presence of one full bond is preferred over two half bonds (Peierls distortion). However, the Li_2Sb structure proves that the energetic differences may be very small, since both alternatives exist in this same structure − as they do in $MoSb_2S$. Also, the differences between $MoSb_2S$ (one linear equidistant, thus an undistorted chain is present) and $MoSb_2Se$ are reminiscent of those between the high- and low-temperature form of $LaSiAs_3$.[23] In this arsenide, an almost square-planar, i.e. undistorted, As layer (with intermediate As−As bonds of 3.01 and 3.05 Å) is present in the high-temperature modification, resembling the $MoSb_2S$ case. This As layer is transformed into zigzag chains in the low-temperature modification (thus resembling the $MoSb_2Se$ case), with short and long As−As distances of alternating 2.56 and 3.52 Å along [100] and 2.76

and 3.29 Å along [010]. In analogy, one can consider $MoSb_2Se$ as the distorted variant of $MoSb_2S$.

However, even if the differences are subtle, why is there no undistorted Sb chain in $MoSb_2Se$, but one in $MoSb_2S$? We speculate that this is due to the matrix effect imposed by the larger chalcogen atom Se, which would make the half bonds longer than in $MoSb_2S$ as reflected in the longer *b* axis of $MoSb_2Se$, namely 3.25 Å compared to 3.19 Å.

The formal charges of each atom in $MoSb_2S$ may be assigned qualitatively based on the Zintl−Klemm concept.[24,25] Among these elements, the electronegativity of sulfur is the largest on any electronegativity scale, and the distances between two nearest S atoms fall in the range of 3.2−3.5 Å, which are normal van der Waals distances. Then, the S atom can be treated as S^{2-} ions. The short Mo−Mo contacts in the Mo zigzag chain suggest a d^2 configuration, that is Mo^{4+}, which is the preferred valence-electron configuration for the transition metal atom zigzag chain. The analogous assignments for MoS_2 and $MoTe_2$ result in $(Mo^{4+})(S^{2-})_2$ and $(Mo^{4+})(Te^{2-})_2$, respectively. The formal charge of each Sb atom is assigned based on the $(8 - N)$ rule, with N = number of full Sb−Sb bonds. Therefore, the Sb atom on the MoSbS layer is Sb^{2-} (one full bond, thus $N = 1$, ergo $8 - N = 7$ valence electrons), and the Sb atom of the zigzag chain is Sb^0 (three full bonds, $N = 3$). The Sb atom from the ladder carries the same charge (i.e. 0), since it comprises two full and two half bonds. We therefore arrive at an electron-precise formula, that is $Mo^{4+}Sb^0Sb^{2-}S^{2-}$, which in general implies that semiconducting properties are possible. In this case, however, semiconducting properties are unlikely due to the presence of other intermediate Sb−Sb interactions (3.18−3.20 Å) within the MoSbS layer. These increase N of the intralayer Sb atom, and thus decrease the formal charge to $(2 - x)-$ with $x < 1$, resulting in the more accurate formulation $Mo^{4+}Sb^0Sb^{(2-x)-}S^{2-}(e^-)_x$ that hints towards metallic properties.

Electronic Structure

Theoretical band calculations using the LMTO method were carried out to study the electronic structure of $MoSb_2S$. The band structure of $MoSb_2S$ is illustrated in Figure 4. Bands cross the Fermi level along each direction, which strongly suggests three-dimensional metallic property. The different orbital contributions can be evaluated by the *fat band* analyses.[26] The results indicate that the orbital contributions near the Fermi level stem mostly from Mo $d_{x^2-y^2}$ and Sb p orbitals from the interlayer Sb atoms (Sb1, Sb5 and Sb6, as emphasized by the fat band representations). The contributions from the S atom are near zero at the Fermi level. Thus, the Mo−Mo and Sb−Sb interactions are likely responsible for the metallic behavior of $MoSb_2S$.

Density of states (DOS) curves for $MoSb_2S$ and the partial projections onto the Mo and Sb atoms are illustrated in Figure 5. The s block of sulfur occurs in the energy window of −13 to −15 eV, and the broad peak between −13 eV and the Fermi level at 0 eV mainly comprises S p, Sb p and Mo d orbitals. There is no band gap, but a pronounced local minimum in the densities of states at the Fermi level.

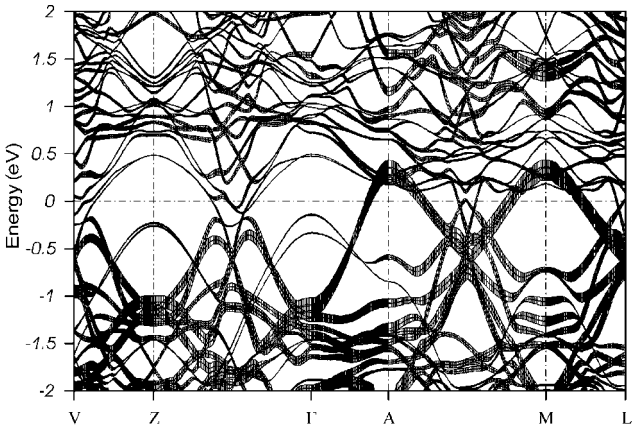

Figure 4. Band structure of $MoSb_2S$; the dashed line denotes the Fermi energy; the interlayer Sb contributions are emphasized

The interatomic interactions in $MoSb_2S$ were analyzed by integrating the area of the COHP curves, resulting in ICOHP values. This is a similar procedure to obtaining the widely used Mulliken overlap populations (MOPs)[27] from the Crystal Orbital Overlap Population (COOP) curves[28] calculated with the Extended Hückel method.[29,30] In contrast to the MOPs, bonding character is reflected in negative ICOHPs. Mo−Mo COHP curves (solid line in Figure 5b) are nearly optimized at the Fermi level E_F (ICOHP = −1.16 eV per bond). A small gap at E_F separates weak antibonding from strong antibonding Mo−Mo states, which suggests that the Mo−Mo bonding will be destabilized by small changes in the valence-electron concentration. The COHP curves of the Mo−S (dotted) and Mo−Sb (dashed) interactions also exhibit a nearly maximized bonding interaction at the Fermi level (ICOHP: Mo−Sb = −1.69; Mo−S = −2.93 eV per bond). All three kinds of interactions shown in Figure 5b comprise zero contributions directly at the Fermi level.

The Sb−Sb interactions are illustrated in Figure 5c for two kinds of Sb−Sb contacts. The first COHP curve (solid line, I) represents the shorter Sb−Sb contacts < 2.9 Å. Almost no antibonding states are filled, the interactions are almost optimized at the Fermi level with an averaged ICOHP value of −1.66 eV per bond. The second COHP curve (dotted line, II) represents Sb−Sb contacts within the MoSbS layer ($3.18 < d_{Sb-Sb} < 3.33$ Å). These interactions exhibit antibonding characters at the Fermi level. The average ICOHP value for these Sb−Sb bonds is −0.31, indicating weaker yet still bonding character. The longer bond of the equidistant ladder of 319 Å (curve III, dashed line) was considered as a half bond, which is reflected in an intermediate ICOHP value of −0.63 eV per bond. These ICOHPs may be compared to those of the two different bonds in elemental antimony, which are −1.63 for the short one of 2.91 and −0.23 eV for the longer one (3.35 Å). For the Sb−Sb bonds of 2.91 and 3.10 Å in Mo_3Sb_7,[31] we calculated similar ICOHPs of −0.79 and −0.40, respectively.

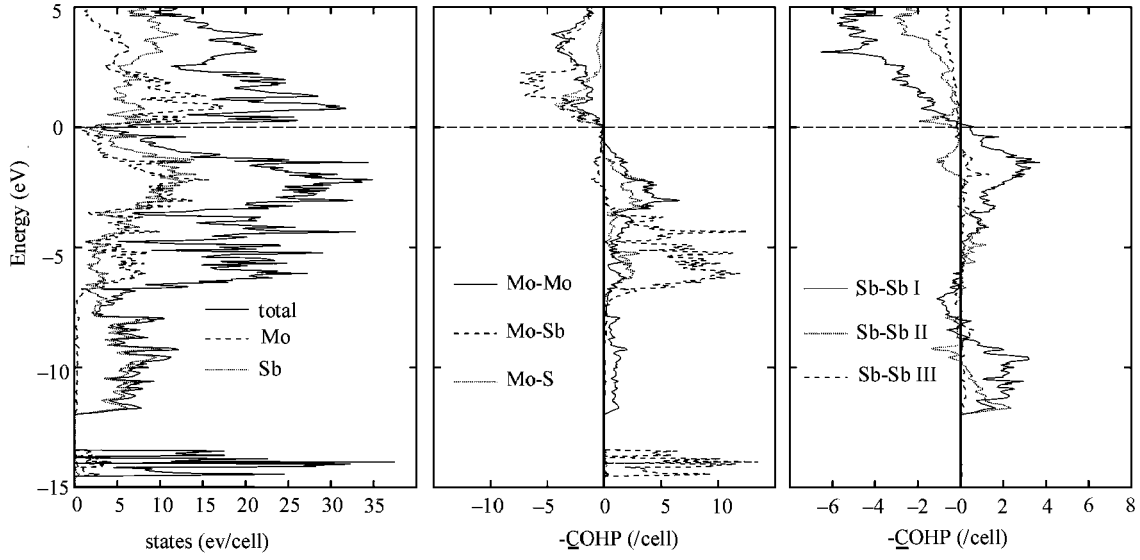

Figure 5. DOS and COHP curves for the $MoSb_2S$; the horizontal dashed line denotes the Fermi energy: a) total DOS (solid line), PDOS from Mo (dashed), Sb (dotted); b) COHP curves for Mo−Mo (solid line), Mo−Sb (dotted), Mo−S (dashed) interactions; c) Sb−Sb contacts (solid line: I, 2.83 < d_{Sb-Sb} < 2.88 Å; dotted line: II, intralayer 3.18 < d_{Sb-Sb} < 3.33 Å, dashed line: III, interlayer 3.19 Å)

Correspondingly, the half bond (3.11 Å) in $Zr_{11}Sb_{18}$ exhibits an ICOHP of −0.49, while the full bonds in KSb have larger ICOHPs of −2.29 and −1.87 eV per bond.[32]

Physical Properties

The temperature-dependent Seebeck coefficient measurement is shown in Figure 6. The Seebeck coefficient drops from −17 μV/K at 300 K to −30 μV/K at 600 K. The negative sign indicates that electrons are the main charge carriers. Typical magnitudes of Seebeck coefficients at 300 K range from a few μV/K for most metals to 10−20 μV/K for some transition metal elements.[1] The observed Seebeck coefficient of $MoSb_2S$ is at the upper end for metallic materials.

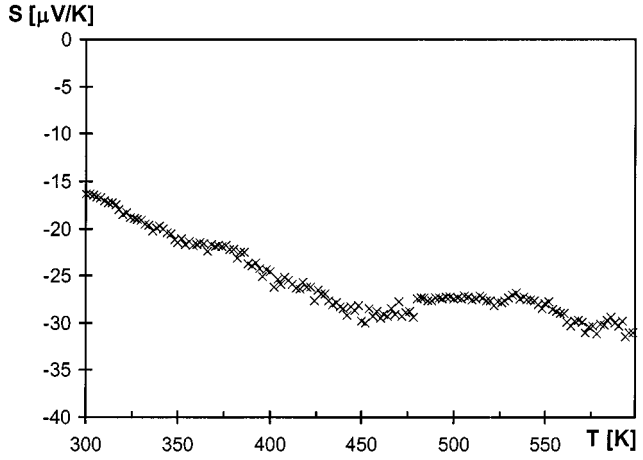

Figure 6. Temperature-dependent Seebeck coefficients of $MoSb_2S$

Conclusion

In summary, the synthesis and characterization of a new ternary compound, $MoSb_2S$, were presented. $MoSb_2S$ crystallizes in a new three-dimensional structure type exhibiting CdI_2-related layers (MoSbS) and Sb columns (*cis-trans* chains and equidistant ladders). The structure comprises strong heteronuclear Mo−S and Mo−Sb bonds, and additional Mo−Mo and Sb−Sb bonds. The Sb atom substructure of $MoSb_2S$ may be considered to be a partly undistorted variant of $MoSb_2Se$. Both antimonide chalcogenides can be formally derived from MoSbS layers topologically equivalent to the β-$MoTe_2$ layers, with additional interlayer Sb atoms. The (formal) intercalation of anionic Sb atoms actually enlarges the octahedral voids between the sheets, thereby rendering an additional intercalation of cations more facile.

$MoSb_2S$ exhibits metallic behavior as predicted by electron counting, electronic structure calculations and confirmed by physical property measurements (Seebeck coefficients). The results from the electronic structure calculations show the smallest number of states directly at the Fermi level; thus, changing the valence-electron concentration is likely to further increase the number of itinerant valence electrons, a disadvantage when looking for thermoelectric materials.

Experimental Section

Synthesis: All starting materials were stored in an Argon-filled glove box. The starting materials were molybdenum (Aldrich, 99.9%), antimony powder (Aldrich, 99.8%, melting point 903 K,

99.5%), sulfur (Aldrich, 99.98%), Mo_3Sb_7 and Sb_2S_3. Mo_3Sb_7 was synthesized by starting from the stoichiometric ratio of Mo/Sb = 3:7 and heating at 973 K for 3 d in an evacuated fused silica tube, whereas Sb_2S_3 was prepared at 773 K within 3 d in an evacuated fused silica tube. Initial reactions were carried out by preparing mixtures in stoichiometric ratios of the elements with a small amount of I_2 as the transport reagent, in a silica tube, sealed under vacuum ($< 10^{-3}$ mbar), and heated at 1073 K for 3 d. Black, needle-shaped crystals of $MoSb_2S$ and mixtures of Sb and binary phases (Mo_3Sb_7, MoS_2) were observed from these reactions. Pure $MoSb_2S$ can be synthesized either by heating stoichiometric amounts of the elements at 873 K for 3 d or annealing binary compounds Mo_3Sb_7 and Sb_2S_3 in a 1:1 ratio at 973 K for 2 d. The purity of $MoSb_2S$ was checked by powder X-ray diffraction and elemental analyses (EDS, see below). The second reaction route (Mo_3Sb_7 + Sb_2S_3) yielded $MoSb_2S$ and elemental antimony, that crystallized on different sides of the reaction container. Higher reaction temperatures (> 1123 K) for both reaction routes led to the disproportionation of $MoSb_2S$ into MoS_2, Mo and Sb. $MoSb_2S$ is stable in air for at least two weeks.

Structure Determination: Needle-shaped crystals for single-crystal X-ray diffraction experiments were selected under an optical microscope and then mounted on glass fibers. Single-crystal X-ray diffraction data were collected with the use of graphite-monochromatized Mo-K_α radiation (λ = 0.71073 Å) at 298(2) K with a Bruker APEX CCD diffractometer. The crystal-to-detector distance was 4.550 cm. Data were collected by a scan of 0.3° in ω groups of 606 frames each at φ settings of 0°, 60°, 120°. The exposure time was 120 s/frame. The 2θ values varied between 3° and 70°. The data were corrected for Lorentz and polarization effects. Absorption corrections were based on fitting a function to the empirical transmission surface as sampled by multiple equivalent measurements.[33] Diffraction peaks obtained from all frames of reciprocal space images were used to determine the unit cell parameters. Initially, the data revealed a primitive unit cell similar to the one of $MoSb_2Se$ and additional weak reflections, which suggested a supercell. The unit cell parameters of $MoSb_2S$ indicated monoclinic symmetry, as later proven by a comparison of symmetry-equivalent reflections (R_{int} = 0.043). The systematic absences revealed *C*-centering. Therefore, the space group *C*2/*m* was chosen for subsequent structural analyses. The structure model was obtained by direct methods and refined by full-matrix least-squares refinement based on F^2 with the SHELXTL5.12 package.[34] Table 1 summarizes the crystallographic data of $MoSb_2S$. Table 2 lists selected interatomic distances. Further details of the crystal-structure investigations may be obtained from the Fachinformationszentrum Karlsruhe, 76344 Eggenstein-Leopoldshafen, Germany, on quoting the depository number CSD-412092. All Mo and S atoms exhibit reasonable thermal displacement parameters. However, the Sb5 and Sb6 atoms show 2−3 times higher thermal displacement parameters along each main direction, which might suggest an even higher order of supercell or lower symmetry. However, lowering the symmetry, for example by refining in C_2 or *Cm*, did not result in any improvements. Also, we found no evidence for the existence of a higher superstructure.

Elemental Analysis: Energy dispersive spectroscopy (EDS, LEO 1050) was performed on the crystalline and powdered samples. The Mo/S ratio could not be determined due to the severe overlap of the peaks of Mo (L_α = 2.293 eV) and S (K_α = 2.307 eV). No impurities of other elements (like iodine, silicon or oxygen) were detected.

Table 1. Crystal data and conditions of data collection for $MoSb_2S$

Refined composition	$MoSb_2S$
Instrument	Smart APEX CCD
Molecular mass	371.5
Crystal size [mm]	0.16 × 0.04 × 0.01
Space group, *Z*	*C*2/*m*, 16
a [Å]	36.157(3)
b [Å]	6.3823(5)
c [Å]	6.5379(5)
β [°]	95.093(2)
V [Å^3]	1502.8(2)
$2\theta_{max}$	34.99°
Reflections collected	12316
Independent, observed reflections (R_{int})	3506, 1553 (0.043)
$d_{calcd.}$ [g/cm^3]	6.568
Absorption coeff. [mm^{-1}]	17.86
Transmission range	0.82−1.0
Temperature [K]	298(2)
$R1$[a], $wR2$ [$I > 2\sigma(I)$]	0.035, 0.059
Goodness-of-fit on F^2	0.80
Δρ(max/min) [e/Å^3]	2.54/−2.53

[a] $R1 = \Sigma||F_o| - |F_c||/\Sigma|F_o|$; $wR2 = [\Sigma[w(F_o^2 - F_c^2)^2]/\Sigma[w(F_o^2)^2]]^{1/2}$.

Table 2. Selected bond lengths [Å] for $MoSb_2S$

Sb1	Sb1	2.839(1)	Sb5	Sb5	2.853(4)
	Sb1	2.878(3)		Sb6	3.1912(3)
	Sb3	2.844(2)			
Sb2	Sb3	3.3294(7)	Mo1	Mo2	2.7650(9)
	Sb4	3.1912(2)		Mo3	3.1912(3)
	Sb5	2.841(2)		S2	2.382(4)
	Mo1	2.840(2)		S3	2.390(5)
	Mo2	2.823(2)	Mo2	Mo2	3.188(1)
Sb3	Mo1	2.826(2)		Mo2	3.194(1)
	Mo2	2.844(2)		Mo3	2.7596(9)
	Mo3	2.824(2)		S1	2.382(4)
	Sb3	3.1846(9)		S2	2.389(5)
	Sb3	3.1977(9)		S3	2.381(4)
	Sb4	3.3283(7)	Mo3	S1	2.388(5)
				S2	2.380(4)
Sb4	Sb6	2.842(2)	S1	S3	3.1912(3)
	Mo2	2.823(2)	S2	S2	3.188(3)
	Mo3	2.846(2)		S2	3.195(3)

Thermopower Measurements: Seebeck coefficients were determined on a cold-pressed bar by a commercial thermopower measurement apparatus (MMR Technologies) in the temperature range of 300 to 600 K, using Constantan as an internal standard. Silver paint (AMI DODUCO Technology) was used to create electric contacts.

Electronic Structure Calculations: The tight-binding LMTO (Linear Muffin Tin Orbitals)[35−37] band calculations were carried out in order to understand the electronic structure of $MoSb_2S$. The integration in *k* space was performed by an improved tetrahedron method[38] on a grid of 16 × 16 × 8 irreducible *k* points of the first Brillouin zone (i.e. 554 of 2048 *k* points). We analyzed the electronic structure by extracting information from the band structure, Densities of states (DOS), and Crystal Orbital Hamiltonian Population curves (COHP).[39]

Acknowledgments

Financial support from the Canadian Foundation for Innovation, the Ontario Innovation Trust, the Materials Manufacturing Ontario, the Province of Ontario, and the National Science and Engineering Research Council of Canada is appreciated.

[1] D. M. Rowe, *CRC Handbook of Thermoelectrics*, CRC Press, Boca Raton, FL, **1995**.
[2] D.-Y. Chung, T. Hogan, P. Brazis, M. Rocci-Lane, C. Kannewurf, M. Bastea, C. Uher, M. G. Kanatzidis, *Science (Washington, D. C.)* **2000**, *287*, 1024.
[3] T. M. Tritt, M. G. Kanatzidis, G. D. Mahan, H. B. J. Lyon, in *Materials Research Society Symposium Proceeding*, Materials Research Society, Warrendale, PA, **1999**, vol. 545.
[4] B. C. Sales, D. Mandrus, R. K. Williams, *Science* **1996**, *272*, 1325.
[5] F. J. DiSalvo, *Science* **1999**, *285*, 703.
[6] H. Kleinke, *Chem. Commun. (Cambridge)* **2000**, 1941.
[7] B. E. Brown, *Acta Crystallogr.* **1966**, *20*, 268.
[8] A. Brown, *Nature* **1965**, *206*, 502.
[9] K. D. Bronsema, J. L. De Boer, F. Jellinek, *Z. Anorg. Allg. Chem.* **1986**, *540*, 15.
[10] P. Villars, L. D. Calvert, *Pearson's Handbook of Crystallographic Data for Intermetallic Phases*, 2nd ed., ASM International, Metals Park, OH, **1991**.
[11] L. Pauling, *The Nature of the Chemical Bond*, 3rd ed., Cornell University, Ithaca, NY, **1948**.
[12] W. Hönle, H.-G. von Schnering, *Z. Kristallogr.* **1981**, *155*, 307.
[13] N. Korber, F. Richter, *Angew. Chem. Int. Ed. Engl.* **1997**, *36*, 1512.
[14] U. Bolle, W. Tremel, *J. Chem. Soc., Chem. Commun.* **1992**, 91.
[15] H. Holseth, A. Kjekshus, *Acta Chem. Scand.* **1969**, *23*, 3043.
[16] H. Kleinke, *Eur. J. Inorg. Chem.* **1998**, 1369.
[17] H. Kleinke, *Chem. Commun. (Cambridge)* **1998**, 2219.
[18] M. J. Ferguson, R. W. Hushagen, A. Mar, *J. Alloys Compd.* **1997**, *249*, 191.
[19] H. Kleinke, *Chem. Soc. Rev.* **2000**, *29*, 411.
[20] G. Papoian, R. Hoffmann, *J. Am. Chem. Soc.* **2001**, *123*, 6600.
[21] G. A. Papoian, R. Hoffmann, *Angew. Chem. Int. Ed.* **2000**, *39*, 2409.
[22] W. Müller, *Z. Naturforsch., Teil B* **1977**, *32*, 357.
[23] H. Hayakawa, S. Ono, *J. Less-Common Met.* **1988**, *144*, 177.
[24] W. Klemm, *Z. Anorg. Allg. Chem.* **1941**, *247*, 1.
[25] E. Zintl, *Angew. Chem.* **1939**, *1*, 52.
[26] O. Jepsen, O. K. Andersen, *Z. Phys.* **1995**, *97*, 25.
[27] R. S. Mulliken, *J. Chem. Phys.* **1955**, *23*, 2343.
[28] T. Hughbanks, R. Hoffmann, *J. Am. Chem. Soc.* **1983**, *105*, 3528.
[29] R. Hoffmann, *J. Chem. Phys.* **1963**, *39*, 1397.
[30] M.-H. Whangbo, R. Hoffmann, *J. Am. Chem. Soc.* **1978**, *100*, 6093.
[31] E. Dashjav, A. Szczepenowska, H. Kleinke, *J. Mater. Chem.*, in press.
[32] I. Elder, C.-S. Lee, H. Kleinke, *Inorg. Chem.*, in press.
[33] *SAINT Version 4*, Siemens Analytical X-ray Instruments Inc., Madison, WI., **1995**.
[34] *SHELXTL Version 5.12, Reference Manual*, Siemens Analytical X-ray Systems, Inc, Madison, WI, **1996**, **1995**.
[35] U. van Barth, L. Hedin, *J. Phys. C* **1971**, *4*, 2064.
[36] O. K. Andersen, *Phys. Rev. B* **1975**, *12*, 3060.
[37] H. L. Skriver, *The LMTO Method*, Springer, Berlin, **1984**.
[38] P. E. Blöchl, O. Jepsen, O. K. Andersen, *Phys. Rev. B: Condens. Matter* **1994**, *49*, 16223.
[39] R. Dronskowski, P. E. Blöchl, *J. Phys. Chem.* **1993**, *97*, 8617.

Received September 13, 2001
[I01360]